Comput Geosci (2015) 19:479–496
DOI 10.1007/s10596-014-9432-0

ORIGINAL PAPER

# A benchmark for microbially mediated chromium reduction under denitrifying conditions in a biostimulation column experiment

**Sergi Molins · Janek Greskowiak · Christoph Wanner · K. Ulrich Mayer**

Received: 13 January 2014 / Accepted: 16 June 2014 / Published online: 18 September 2014


**Abstract** Bioremediation efforts in aquifers contaminated with redox-sensitive contaminants often rely on in situ reductive immobilization. The bioremediation treatment usually involves injection of organic carbon into the subsurface (e.g., acetate) to stimulate the growth of indigenous bacteria that mediate the relevant redox processes that immobilize the target contaminant. Batch and flow-through column experimental studies are conducted to elucidate reaction networks associated with specific electron acceptor pathways and/or specific bacterial isolates. The proposed benchmark involves the simulation of microbially mediated chromium reduction under denitrifying conditions in biostimulated batch and flow-through column experiments. Simulated reactive processes include multicomponent aqueous complexation, kinetically controlled mineral precipitation and dissolution, biologically mediated reactions, and biomass growth and decay. The focus of the benchmark problem set is on the simulation of microbially mediated redox reactions with the explicit inclusion of the microbial community dynamics and the impacts on reaction rates. Rate expressions for microbially mediated redox reactions include kinetic limitations (Monod and inhibition terms) as well as thermodynamic limitations. Both catabolic (energy) and anabolic pathways (biomass growth) are considered in the microbially mediated reactions. Microbial biomass is assumed to be bound to the sediment (non-planktonic). Any reactive transport model used to reproduce results of this benchmark problem must be capable of simulating multicomponent aqueous complexation, kinetically controlled mineral precipitation and dissolution and kinetically controlled aqueous reactions. Though convenient, it is not necessary to allow for specific stoichiometric relationships for catabolic and anabolic pathways; only the overall reaction stoichiometry is used. Rate expressions for microbially mediated reaction must include a rate constant, the biomass concentration, and a number of Monod and inhibition terms. To ensure that the results presented in this paper were the correct solutions to the problems posed, the general-purpose reactive transport codes CrunchFlow, PHT3D, ToughReact, and MIN3P were used to perform the simulations. In general, results obtained with all codes show excellent agreement.

**Keywords** Reactive transport modeling · Microbially mediated reduction · Denitrification · Chromium reduction · Biomass · Benchmark

**Electronic supplementary material** The online version of this article (doi:10.1007/s10596-014-9432-0) contains supplementary material, which is available to authorized users.

S. Molins (✉) · C. Wanner
Earth Sciences Division, Lawrence Berkeley National Laboratory, One Cyclotron Rd, MS 74R316C, Berkeley, CA 94720, USA
e-mail: smolins@lbl.gov

C. Wanner
e-mail: cwanner@lbl.gov

J. Greskowiak
Department of Biology and Environmental Science, Carl von Ossietzky Universität Oldenburg, Oldenburg, Germany
e-mail: janek.greskowiak@uni-oldenburg.de

K. U. Mayer
Department of Earth, Ocean and Atmospheric Sciences, University of British Columbia, Vancouver, BC, Canada
e-mail: umayer@eos.ubc.ca

## 1 Introduction

Contamination of groundwater by toxic metals is widespread at many sites around the world. Bioremediation efforts in aquifers contaminated with redox-sensitive contaminants such as chromium often rely on in situ reductive immobilization. The bioremediation treatment usually involves injection of organic carbon into the subsurface to stimulate the growth of indigenous bacteria that mediate the relevant redox processes that immobilize the target contaminant. For example, during biostimulation, the soluble and toxic hexavalent form of chromium is reduced to the less soluble and less toxic Cr(III), which tends to form oxides or hydroxides at pH values larger than 5 [16]. In field-scale experiments, the electron donor is injected for limited periods of time, the length of which affects the primary controls on the removal of toxic metals from groundwater [25]. In the transient regime, consideration of biomass dynamics is important in that growth and accumulation of biomass contribute to increasing reaction rates over time (e.g., [11]). The dynamics of biomass growth in cyclically stimulated aquifers has also been shown to lead to hysteretic responses to injection of carbon sources [6].

Numerous experimental and field studies have been conducted to understand the potential effectiveness of bioremediation treatments [2, 5, 7, 24, 25]. Depending on the number of electron acceptors present in situ, a complex series of biogeochemical reactions can occur with their products further reacting to form mineral precipitates, making it difficult to unravel the biogeochemical reaction network. As a result, laboratory experimental studies and batch and flow-through column experiments have often focused on specific electron acceptor pathways and/or specific bacterial isolates [2, 3, 9]. Typically, this approach is not possible in the field due to chemical and biological heterogeneity.

Process-based biogeochemical reactive transport modeling has been used as a tool in identifying and quantifying the critical and interrelated microbial metabolic and geochemical mechanisms associated with reductive immobilization of contaminants [6, 10, 11, 27]. In many cases, laboratory studies focusing on single electron acceptor pathways and specific bacterial isolates are used to calibrate parameters in the models that can be used later in field-scale models [1, 4].

The objective of this work is to present a benchmark problem for the simulation of redox problems in batch and flow-through reactors that focuses on the biomass dynamics that occurs in the transient stages of an injection of an organic carbon source. The problem uses well-established formulations that are based on (1) mass balance that poses limitations on biomass growth depending on both substrate and nutrient availability and (2) Monod-type expressions. This makes this problem potentially addressable by most general-purpose reactive transport codes.

The problem set presented here includes the simulation of microbially mediated chromium reduction under denitrifying conditions in batch experiments and in a biostimulation column experiment. The benchmark problem set does not reproduce specific quantitative results of any study. However, it attempts to synthesize the qualitative behaviors observed in a number of previous experimental and modeling studies [1, 4, 9]. In particular, it captures the co-metabolic reduction of chromium under denitrifying conditions observed in a batch experiment under no-growth conditions by Han et al. [9]. Further, it follows the approach of Andre et al. [1] where parameters calibrated using batch denitrification experimental results were used to conduct the simulation of flow-through column experiments. Of particular interest is to capture the dynamics of biomass growth and their effect on overall microbially mediated reaction rates, such as those observed by Andre et al. [1] and Clement et al. [4]. The parameters used in the problem set are consistent with those employed in previous studies.

To ensure that results presented here accurately represent the solution to the problem and are reproducible by other simulators, four different reactive transport codes have been used to simulate the problem set by the four authors of this manuscript. These codes are CrunchFlow [11], PHT3D [15], ToughReact [26], and MIN3P [13, 14].

## 2 Conceptual and mathematical model

The model includes microbially mediated reactions, aqueous kinetic reactions, and aqueous complexation reactions. These reactions affect the mass of the chemical species considered in the geochemical system; thus, the mass balance equation is the governing equation of the model. When transport processes are considered, advective and diffusive terms also contribute to the mass balance equations.

### 2.1 Microbially mediated reactions

Microbial cells use the energy that is released during the electron transfer from the electron donor to the acceptor in reduction-oxidation reactions. The approach of [17] is based on the stoichiometry of the reaction, where microorganisms appear as a product of the reaction, in addition to being the catalysts of the reaction. A portion $f_e^0$ of the electrons from the substrate is transferred to the electron acceptor to provide energy for conversion of the other portion of electrons ($f_s^0$) into microbial cells, satisfying $f_e^0 + f_s^0 = 1$. The overall stoichiometry of the microbially mediated reaction is thus constructed by adding the catabolic (energy)

and anabolic (biomass growth) pathways weighted by these portions:

$$0 = \sum_k^{N_c} \nu_{jk}^e A_k \quad (1)$$

$$0 = \sum_k^{N_c} \nu_{jk}^s A_k \quad (2)$$

$$0 = \sum_k^{N_c} (f_e^0 \nu_{jk}^e + f_s^0 \nu_{jk}^s) A_k = \sum_k^{N_c} \nu_{jk}^b A_k \quad (3)$$

where $N_c$ is the number of primary species; $A_k$ is the chemical formula of the primary species; $\nu_{jk}^e$ and $\nu_{jk}^s$ are the stoichiometric coefficients of the primary species in the catabolic and anabolic pathways, respectively, for the $j$-th reaction; and $\nu_{jk}^b$ are the stoichiometric coefficients in the overall redox reaction. In the model proposed here, the values of $f_e^0$ and $f_s^0$ are constant throughout the simulations, and therefore, only $\nu_{jk}^b$ needs to be used. Table 1 presents the stoichiometry of the catabolic and anabolic pathways, as well as the overall reactions used in the model following the convention of [17], where reactions are written per electron equivalent transferred (i.e. 1 mol reaction = 1 $e^-$ equivalent). The stoichiometric formula $C_5H_7O_2N$ is commonly used in modeling applications to represent biomass and is also used here. Denitrification processes that reduce $NO_3^-$ according to a series of catabolic reactions are included in the model (R1 and R2 Table 1):

$$NO_3^- \rightarrow NO_2^- \rightarrow N_2$$

Two anabolic pathways are considered, one that uses $NH_4^+$ as nitrogen source for biomass growth (R3, dissimilatory pathway) and the other that uses $NO_2^-$ as nitrogen source (R4, assimilatory pathway). As a result, four overall reactions for denitrification are considered (R5–R8, Table 1). In addition, the reaction network includes the catabolic pathways of Cr(VI) reduction (anabolic pathways are neglected). Each Cr(VI) reduction step is associated with a denitrification step (R9–R10, Table 1).

A Monod-type expression is used to calculate the rate for the microbially mediated reactions. In units of moles of reaction per liter per second for the rate of reaction $j$ is:

$$r_j = \mu_j B \frac{c_D}{c_D + K_D} \frac{c_A}{c_A + K_A} \frac{K_H}{c_H + K_H} F_T \quad (4)$$

where $\mu_j$ is the specific rate constant (mol cell$^{-1}$ s$^{-1}$); $B$ is the concentration (cells L$^{-1}$); $c_D$, $c_A$, and $c_H$ are the concentration of the electron donor, acceptor and inhibitor

**Table 1** Stoichiometry of microbially mediated reactions

| Number | Reaction | Primary species | | | | | | | | | |
|---|---|---|---|---|---|---|---|---|---|---|---|
| | | $H^+$ | $HCO_3^-$ | Acetate | $NO_3^-$ | $NO_2^-$ | $N_2$(aq) | $NH_4^+$ | $CrO_4^{--}$ | $Cr^{+++}$ | $C_5H_7O_2N$ |
| R1 | Catabolic | | | | | | | | | | |
| | $NO_3^- \rightarrow NO_2^-$ | 0.125 | 0.25 | −0.125 | −0.5 | 0.5 | 0 | 0 | 0 | 0 | 0 |
| R2 | Catabolic | | | | | | | | | | |
| | $NO_2^- \rightarrow N_2$(aq) | −0.20833 | 0.25 | −0.125 | 0 | −0.33333 | 0.166667 | 0 | 0 | 0 | 0 |
| R3 | Anabolic – dissiml. | | | | | | | | | | |
| | Acetate $\rightarrow C_5H_7O_2N$ | −0.075 | 0 | −0.125 | 0 | 0 | 0 | −0.050 | 0 | 0 | 0.050 |
| R4 | Anabolic – assimil. | | | | | | | | | | |
| | Acetate $\rightarrow C_5H_7O_2N$ | −0.105769 | 0.057692 | −0.125 | 0 | −0.038461 | 0 | 0 | 0 | 0 | 0.038461 |
| R5 | Overall fe = 0.6 | | | | | | | | | | |
| | $NO_3^- \rightarrow NO_2^-$ | 0.045 | 0.15 | −0.125 | −0.3 | 0.3 | 0 | −0.02 | 0 | 0 | 0.02 |
| R6 | Overall fe = 0.6 | | | | | | | | | | |
| | $NO_2^- \rightarrow N_2$(aq) | −0.155 | 0.15 | −0.125 | 0 | −0.2 | 0.1 | −0.02 | 0 | 0 | 0.02 |
| R7 | Overall fe = 0.6 | | | | | | | | | | |
| | Assimilatory | | | | | | | | | | |
| | $NO_3^- \rightarrow NO_2^-$ | 0.032692 | 0.173077 | −0.125 | −0.3 | 0.284615 | 0 | 0 | 0 | 0 | 0.015385 |
| R8 | Overall fe = 0.6 | | | | | | | | | | |
| | Assimilatory | | | | | | | | | | |
| | $NO_2^- \rightarrow N_2$(aq) | −0.167308 | 0.173077 | −0.125 | 0 | −0.215385 | 0.1 | 0 | 0 | 0 | 0.015385 |
| R9 | Cr reduction | | | | | | | | | | |
| | ($NO_3^-$) | −1.54167 | 0.25 | −0.125 | 0 | 0 | 0 | 0 | −0.33333 | 0.333333 | 0 |
| R10 | Cr reduction | | | | | | | | | | |
| | ($NO_2^-$) | −1.54167 | 0.25 | −0.125 | 0 | 0 | 0 | 0 | −0.33333 | 0.333333 | 0 |

*Stoichiometric coefficients for products > 0 and for reactants < 0

(mol $L^{-1}$), respectively; $K_D$, $K_A$, and $K_H$ are the half-saturation constants for the electron donor, acceptor and inhibitor (mol $L^{-1}$), respectively; and $F_T$ is the thermodynamic limitation term as described by Jin and Bethke (2005). Under denitrifying conditions, reaction rates are typically not thermodynamically limited [1] and therefore the term $F_T$ does not play a role in the model presented here, i.e. $F_T = 1$

Since Cr(VI) reduction is directly associated with denitrification, the biomass of denitrifiers $B$ (4) is also used to calculate the reaction rate for Cr(VI) reduction. The contribution of each reaction to the mass balance of the biomass component is calculated as the product of the reaction rate ($r_j$) times the stoichiometric coefficient for biomass ($C_5H_7O_2N$). This procedure accounts for bacterial growth and at the same time for potential limiting factors on growth based on the availability of nutrients that appear as reactants (R5–R8, Table 1). Biomass decay is calculated with a first-order rate expression:

$$r_{\text{decay}} = -bB \tag{5}$$

Cryptic growth where death cells are used as substrate for additional biomass growth is not considered in the model. Biomass is assumed to be present only as immobile species; thus, biomass decay, if considered, is the only process that accounts for biomass removal.

## 2.2 Aqueous equilibrium and mineral precipitation and dissolution

Aqueous equilibrium reactions are described using an equilibrium formulation using the law of mass action. These additional constraints given by the $N_x$ aqueous complexation reactions are used to define the $N_c$ components for which the mass balance equations are solved [12, 18]. A total of 33 aqueous species and 20 aqueous complexation reactions are considered (Tables 3 and 4 of the Appendix). Activity coefficients of aqueous species are calculated using a Debye-Huckel model (Table 9 of the Appendix). Including the biomass component, the geochemical system contains 14 component species: $H^+$, $Na^+$, $Ca^{2+}$, $Cl^-$, $HCO_3^-$, acetate, $NO_3^-$, $NO_2^-$, $N_2$(aq), $NH_4^+$, $O_2$(aq), $CrO_4^{2-}$, $Cr^{3+}$, and $C_5H_7O_2N$ (Table 3 of the Appendix).

Precipitation and dissolution reaction rates are calculated with a kinetic formulation based loosely on the transition state theory at 25 °C:

$$r_m = -k_m A_s \left(1 - \frac{Q}{K_s}\right) \tag{6}$$

where $k_m$ is the rate constant (mol $m^{-2}$ $s^{-1}$), $A_s$ is the bulk mineral surface area ($m^2$ $m^{-3}$ bulk), $Q$ is the ion activity product and $K_s$ is the solubility constant. Two minerals are included in the simulations: $CaCO_3$ as primary mineral and $Cr(OH)_3$ as secondary mineral that precipitates out of solution when Cr(VI) is reduced to Cr(III). Parameters for these minerals are given in Table 5 of the Appendix. The bulk surface area for calcite is kept constant, and the one for $Cr(OH)_3$ is calculated according to the following:

$$A_s = A_{\text{specific}}\, \phi_{Cr(OH)_3}\, \rho_{Cr(OH)_3} \tag{7}$$

where $A_{\text{specific}}$ is the specific surface area ($m^2$ $g^{-1}$), $\phi_{Cr(OH)_3}$ is the mineral volume fraction ($m^3$ mineral $m^{-3}$ bulk) and $\rho_{Cr(OH)_3}$ is the solid density ($9.281 \times 10^6$ g $m^{-3}$ mineral). Porosity changes due to precipitation of $Cr(OH)_3$ and accumulation of biomass are neglected.

## 2.3 Mass balance

In addition to reactive processes, transport of geochemical species is considered in the mass balance of species in the flow-through simulations. In the batch simulations, the transport terms are neglected. The multicomponent reactive one-dimensional transport (advection and diffusion) of component $k$ is described by the following mass balance equation:

$$\frac{\partial}{\partial t}(\phi \rho u_k) + \nabla \cdot (\rho \mathbf{q} u_k) - \nabla \cdot (\rho D \nabla u_k) = R_k \tag{8}$$

where $\rho$ is the fluid density, $\phi$ is the porosity, $\mathbf{q}$ is the Darcian flux, and $D$ is the combined molecular diffusion coefficient. Dispersion is not considered. The total molal concentration of component $k$, $u_k$ (moles per kilogram of $H_2O$), is the sum of the concentrations of the individual species at chemical equilibrium with the component weighted by the appropriate stoichiometric coefficient. The term $R_k$ (moles per unit volume rock per unit time) is the total reaction rate affecting the mass of component $k$ in solution.

## 2.4 Boundary conditions

In the transport model for the flow-through simulations, flow is one-dimensional, uniform, and kept constant through the simulation time. At the inlet boundary, constant mass influxes for all components are applied to the first cell of the domain. These mass fluxes are the product of the one-dimensional flow rate and a set of fixed concentrations of each component species. This boundary condition is equivalent to injecting an experimentally prepared stock solution into a flow-through column experiment. The outlet is a free exit boundary

(no diffusion, only advection of the concentrations in the domain).

## 3 Numerical model and codes

The multicomponent system of equations expressed by Eq. (8) is non-linear. The global implicit approach (GIA) involves solving the resulting system of non-linear equations simultaneously using a Newton-Raphson system [19]. Operator-splitting (OS) methods solve transport and reactions separately [28]. In this approach, the time-step size is constrained by the Courant criterion, but advective transport can be solved using accurate explicit methods such as the total variation diminishing or TVD [8] that minimize numerical dispersion. Non-linear spatial weighting schemes such as the van Leer flux limiter [22] improve the accuracy of implicit methods versus upstream or centered weighting schemes [21].

The codes that were used to simulate the problem set presented in Section 4 are CrunchFlow [11], PHT3D [15], ToughReact [26], and MIN3P [13, 14]. A summary of the solution approaches and discretization techniques employed in the codes is presented in Table 2. The reader is directed to Steefel et al. [20] and the references above for exploring the specific capabilities available in these models.

## 4 Problem set

The principal problem of this benchmark is the simulation of microbially mediated chromium reduction under denitrifying conditions in a column experiment permeated at a constant flow rate with a solution containing acetate as electron donor, nitrate as electron acceptor, and chromate. The principal problem is constructed with component problems that add incremental levels of complexity and additional processes. This serves to highlight relevant effects of model assumptions when simulating and to test specific model components. For this, a problem set composed of five component problems is proposed, two that do not include transport (Sections 4.1, and 4.2) and three that include transport under different assumptions for biomass growth and decay (Sections 4.3, 4.4, and 4.5). Section 4.5 presents the principal problem. All component problems include all aqueous complexation and mineral reactions presented in Tables 4 and 5 of the Appendix. Rate constants and kinetic parameters for mineral reactions are given in Table 8 of the Appendix. Rate constants and kinetic parameters for microbially mediated reactions are provided in Tables 6 and 7 of the Appendix. Half-saturation constants for the acetate, nitrate, and nitrite are those in the study of Clement et al. [4]. The rate constants for the denitrification reactions fall within the range of rate constants reported by Andre et al. [1] (1–4 $\times$ $10^{-21}$ mol cell$^{-1}$ s$^{-1}$) and Clement et al. [4] (4.56 $\times$ $10^{-19}$ mol cell$^{-1}$ s$^{-1}$). Rate constants for chromium reduction reactions are chosen in relation to denitrification rates so as to reproduce the co-metabolic process described by Han et al. [9], where Cr reduction rates are approximately 3 orders of magnitude slower than denitrifying rates. Sections below outline which redox reactions from Table 1 are used in each case.

### 4.1 No-growth batch simulation (*batch 1*)

This component problem concerns the simulation of an experimental batch system. The experiment is initiated by adding a solution of concentrated cells to a basal medium amended with nitrate, acetate, and chromate (Tables 10, 11 and 12 of the Appendix). Concentrations of nitrate and acetate are 1.5 and 1.0 mmol L$^{-1}$, respectively, near the values used in the experiments by Andre et al. (0.80 and 0.84 mmol L$^{-1}$) [1] and Clement et al. (0.77 and 0.98 mmol L$^{-1}$, for the high-load experiment) [4]. Denitrifying bacterial cells mediate nitrate reduction and chromium

**Table 2** Codes and capabilities

| | CrunchFlow | PHT3D | ToughReact | MIN3P |
|---|---|---|---|---|
| Approach | OS (GIA not used here) | OS (SNIA) | OS | GIA |
| Discretization | Integrated finite differences (finite volumes) | Finite differences | Integrated finite differences (finite volumes) | Integrated finite differences (finite volumes) |
| Flux limiters, total variation diminishing | TVD (in OS) | TVD, various methods of characteristics | | VanLeer flux limiter |

*GIA*: global implicit approach
*OS*: operator splitting
*SNIA*: sequential non-iterative approach

reduction by using acetate as electron donor. This problem represents experiments similar to the cell suspensions of [9] where biomass growth was suppressed by the addition of chloramphenicol. However, the concentration of biomass in the simulations is $10^{-4}$ mol $L^{-1}$ ($5 \times 10^{10}$ cells $L^{-1}$), much lower than that of the cell suspensions of Han et al. [9] and closer to that used by Andre et al. [1] ($10^{10}$ cells $L^{-1}$) and Clement et al. [4] ($3.61 \times 10^{9}$ cells $L^{-1}$). Since biomass growth is not considered, only catabolic pathways are used (i.e., Table 1, R1, R2, R9, R10).

The domain is discretized using a single-grid cell. The simulation is run for 20 days, with an initial time step of $10^{-10}$ days and a maximum time step of 0.1 days. The initial concentrations of all components, species, and biomass are given in Tables 10, 11 and 12 of the Appendix, except for the initial concentration of $NH_4^+$, which is $0.5 \times 10^{-4}$ mol $L^{-1}$.

### 4.2 Biomass growth batch simulation (*batch 2*)

This component problem builds on the processes and parameters of *batch 1*. However, this simulation includes biomass growth by including anabolic pathways in the nitrate and nitrite reduction reactions. The catabolic pathways are also considered. A growth yield of $f_s^0 = 0.4$ is assumed, implying that 40 % of electron equivalents obtained from acetate oxidation is used for biomass growth. The resulting yield for the $NO_3^-$ to $NO_2^-$ step is 0.067 mol biomass $mol^{-1}$ $NO_3^-$, which compares to that used by Clement et al. [4] (0.071 mol biomass $mol^{-1}$ $NO_3^-$). The microbially mediated reactions include nitrate and nitrite reduction (R5 and R6 of Table 1), assimilatory nitrate and nitrite reduction (R7 and R8 of Table 1), and chromium reduction (R9 and R10 of Table 1). Assimilatory reduction is also added to the reaction network, but it does not play a role here. The role of assimilatory pathways is discussed for the principal problem. This problem intends to represent batch experiments similar to [1] where biomass growth in a batch experiment results in increasing denitrification rates with time. Biomass decay is neglected.

The domain is discretized, and time stepping is the same as in batch 1. The initial concentrations of all components, species, and biomass are given in Tables 10, 11 and 12 of the Appendix.

### 4.3 Growth column simulation (*column 1*)

This component problem builds on the processes and parameters of *batch 2* and adds one-dimensional transportto the simulations. The simulation involves a 10-cm-long column continuously treated at a constant flow rate (0.006 cm $min^{-1}$) with a stock solution containing acetate as electron donor, nitrate as electron acceptor, and chromate. Denitrifying bacteria initially uniformly distributed in the soil mediate nitrate reduction and co-metabolic chromium reduction by using acetate as electron donor. The initial concentration of biomass is $5 \times 10^{-5}$ mol $L^{-1}$, and the inlet concentrations of nitrate and acetate are 1.5 and 1.0 mmol $L^{-1}$, respectively. This problem intends to represent column experiment simulations conducted by [1] where biomass growth in a batch experiment results in increasing denitrification rates with time though biomass decay is not considered and the time frame considered is quite different (100 days vs. 200 h in [1]).

The domain is discretized using 100 grid cells of equal length of 0.1 cm with homogeneous porosity equal to 0.4. The simulation is run for 100 days, with an initial time step of $10^{-10}$ days, and a maximum time step is 1 day. The constant flow velocity (Darcy flux) is 0.006 cm $min^{-1}$. The diffusion coefficient for all species is assumed to be $10^{-5}$ $cm^2$ $s^{-1}$.

The concentrations of all component, species and biomass given in Tables 10, 11, 12, 13 and 14 of the Appendix are used as initial conditions and as inlet boundary condition. The same reaction network and kinetic parameters are used as in *batch 2* (Section 4.2).

### 4.4 Growth and decay column simulation (*column 2*)

This component problem builds on the processes and parameters of *column 1* and adds biomass decay according to Eq. (5). The decay parameter $b$ is 0.00432 $day^{-1}$, an order of magnitude smaller than the value of 0.06 $day^{-1}$ used by Clement et al. [4], but within the range of decay rates reported in the modeling studies of Yabusaki et al. [27] and Druhan et al. [6]. This problem intends to represent column experiment simulations conducted by [4] where biomass growth and decay are considered. In the model presented here, biomass detachment is, however, not included, and biomass is assumed to accumulate where it is produced.

### 4.5 Principal problem (*column 3*)

This component problem uses the processes and parameters of *column 2*, but the inflow solution is slightly modified to limit biomass growth as explained below. The stoichiometric relationships in Table 1, R5–R8, are mass balanced such that biomass growth (reaction product) depends on the availability of the reactants. When reaction rates near the inlet of the column are fast due to increasing biomass accumulation Eq. (4), reactants supplied

in stock solution fed into the column are depleted further downstream, and their concentrations become limiting for biomass growth. In these conditions with lack of $NH_4^+$ as nitrogen source for growth, denitrifiers can use $NO_3^-$ and $NO_2^-$ as nitrogen source. This is represented here with reactions R7 and R8 (formed with the anabolic pathway in R4). Assimilatory pathways are assigned slower rate constants given that they are less favorable to denitrifiers. The only difference with respect to column 2 is that the total concentration of $NH_4^+$ in the stock solution was decreased to a value of 0.05 mol $L^{-1}$. This lower concentration causes the nitrite assimilatory pathway (Table 1, R7 and R8) to play a role in slowing down the overall reaction rate.

## 5 Results and discussion

### 5.1 No-growth batch simulation (*batch 1*)

Oxidation of acetate takes place by sequentially using $NO_3^-$ and $NO_2^-$ as electron acceptors. Inhibition of $NO_2^-$ reduction in the presence of $NO_3^-$ and acetate has been observed before [23] and has been modeled here with the inhibition term of Eq. (4) as a function of $NO_3^-$ concentration. Reduction of Cr(VI) is linked to nitrate reduction by including Monod terms for $NO_3^-$ and $NO_2^-$ in two separate pathways associated each to $NO_3^-$ and $NO_2^-$, respectively (R9 and R10, Table 1). As a result, two periods are observed in the reduction of Cr(VI) each related to the main electron acceptor used in acetate oxidation.

Results agree qualitatively with the batch experiments of Han et al. [9] where reactants evolved linearly with time until they were fully consumed (cf. Fig. 1 in [9]). In other words, rates did not change significantly with time because the biomass concentration was constant. In the simulation, Monod terms have very limited influence in the overall evolution and only play a role at very small reactant concentrations. As observed in [9], nitrite consumption does not start until nitrate has been fully consumed.

Results from all codes produce very similar results (Fig. 1), ensuring correctness of this solution. This is important given that implementation of certain processes is different in different codes (e.g., MIN3P, ToughReact, and PHT3D use immobile aqueous species for biomass, while CrunchFlow sets an arbitrarily fast heterogeneous reaction to simulate an immobile biomass component). The most visible differences are in the concentration of $Cr^{3+}$ due to its small numerical values and possible differences in the treatment of reactive surface area of the mineral that controls Cr(III) concentrations in the aqueous phase.

### 5.2 Biomass growth batch simulation (*batch 2*)

Compared to *batch 1*, inclusion of biomass growth results in increasing reaction rates in the batch system due to increasing biomass concentrations (Fig. 2). This is reflected in the curved shape of the concentration evolution (Fig. 2) compared to linear evolution in Fig. 1. Another consequence of growth is consumption of $NH_4^+$, though it does not become limiting to growth at any point (Fig. 2). Contrary to intuition, in spite of increasing rates, complete depletion of $NO_3^-$ is delayed by a day with respect to batch 1. This occurs because for each electron equivalent available from acetate, only 0.6 is used in the catabolic pathway, where $NO_3^-$ is used as electron acceptor. The remaining 0.4 electron equivalents are used for biomass growth. Biomass growth results in faster consumption of the electron donor acetate that becomes depleted short of 20 days and inhibits further reaction progress.

The results agree qualitatively with the experiments and simulation of Andre et al. [1] where increasing denitrification rates are observed in the batch system concurrent with increasing biomass concentrations (cf. Figs. 2, 4, and 5 in [1]).

### 5.3 Growth column simulation (*column 1*)

In the flow-through column simulations, the supply of electron donor, acceptors, and $NH_4^+$ at the inlet end is continuous in time. To observe significant consumption of the target contaminant, e.g., Cr(VI), these experiments rely on biomass growth from an initial biomass that is stimulated with the amendment. In the simulation of column 1, acetate is consumed completely before Cr(VI) has been completely removed from the effluent (Fig. 3). At 100 days, complete consumption of acetate occurs at half the length of the column due to a large accumulation of biomass near the inlet. Biomass accumulation shows a positive feedback where accumulation results in faster rates (4), which in turn result in additional biomass growth and further accumulation (e.g., R5, Table 1). Biomass concentrations at 100 days near the outlet end of the column (length > 5 cm, Fig. 4) reflect earlier growth conditions (no decay is included here). However, biomass in this region is not contributing to the reduction of Cr(VI) because acetate is depleted. Preferential accumulation of biomass near the inlet end of the column also results in accumulation of $Cr(OH)_3(s)$ precipitate in this area (Fig. 4).

The difference in the time scales considered in the simulation as well as additional processes (e.g., pyrite

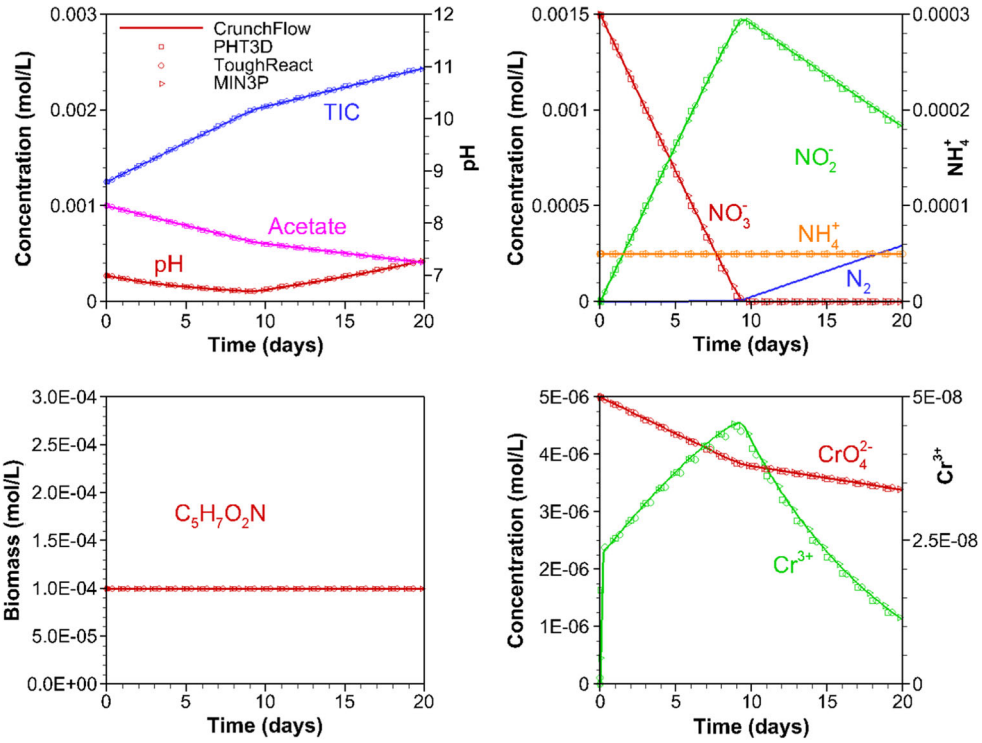


**Fig. 1** Evolution of major components in the simulation of Cr(VI) reduction under denitrifying conditions in a batch system with suppressed biomass growth (*batch 1*)

dissolution/oxidation) not considered here make the results of this simulation not directly comparable to work of Andre et al. [1].

All codes but MIN3P were run using an operator-splitting approach. MIN3P used the van Leer flux limiter [22] and limited the time-step value by the Courant criteria as necessary in the operator-splitting approach. Results show little numerical dispersion with time-dependent and spatial results from all codes showing the same solution to the problem.

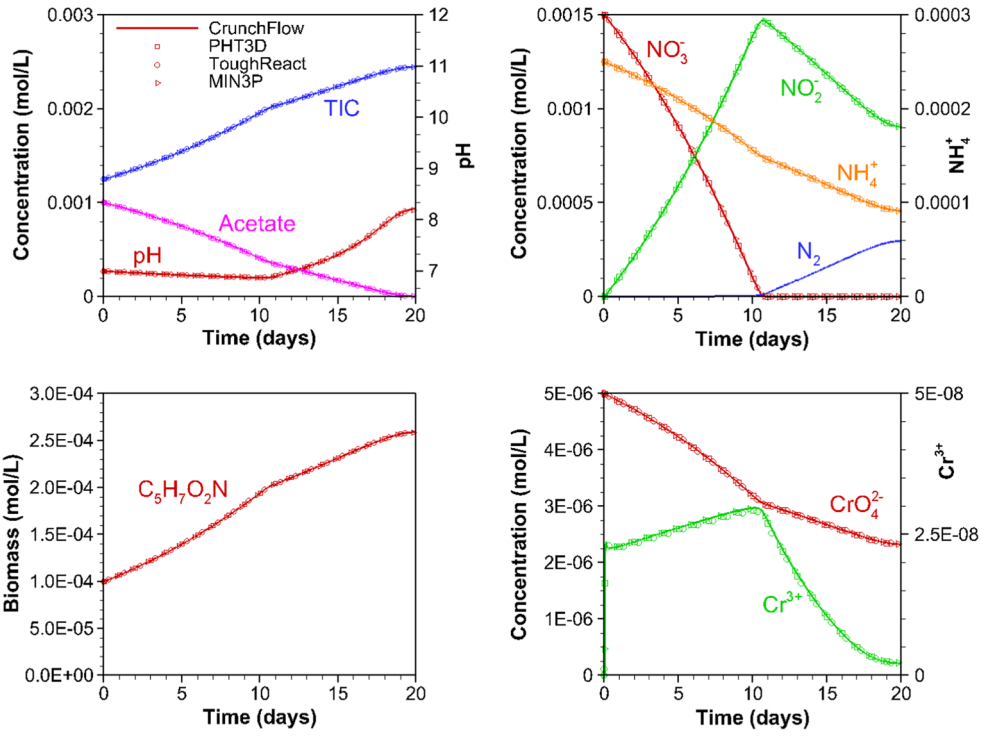


**Fig. 2** Evolution of major components in the simulation of Cr(VI) reduction under denitrifying conditions in a batch system with biomass growth (*batch 2*)

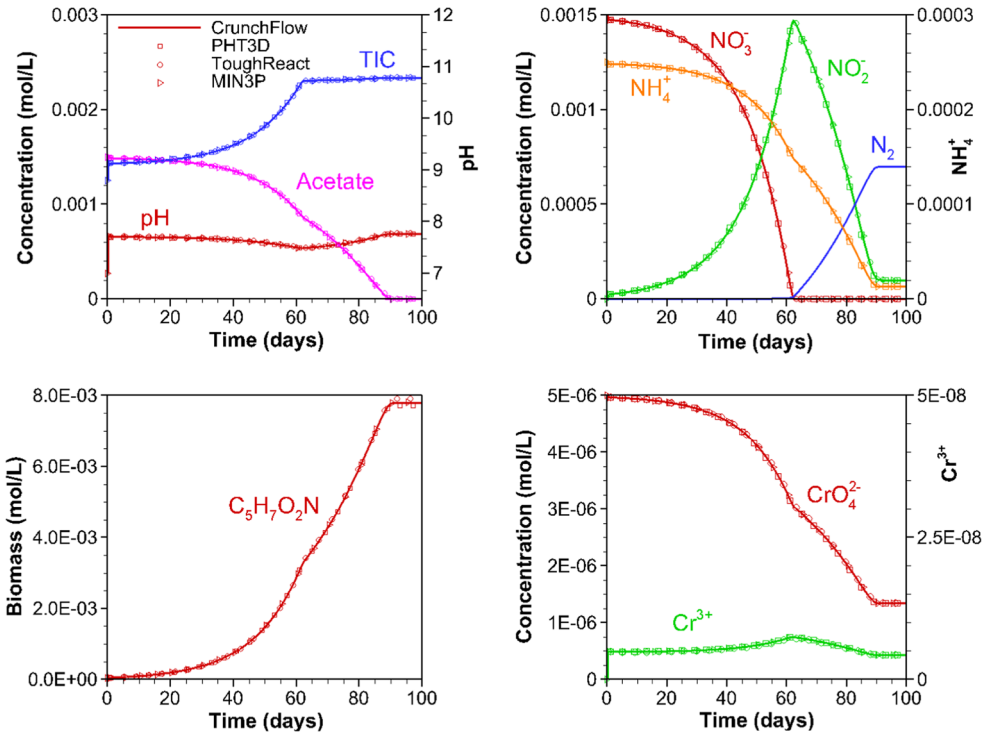


**Fig. 3** Evolution of major components in the simulation of Cr(VI) reduction under denitrifying conditions in a flow-through column with biomass growth (*column 1*)

5.4 Growth and decay column simulation (*column 2*)

Biomass decay has the effect of significantly slowing down redox rates in the column. In *column 2*, acetate is not depleted in the effluent after 100 days, and $NO_3^-$ is completely removed 20 days later than in *column 1* (Fig. 5). Denitrification and Cr(VI) reduction takes place along the full length of the column (Fig. 6), although

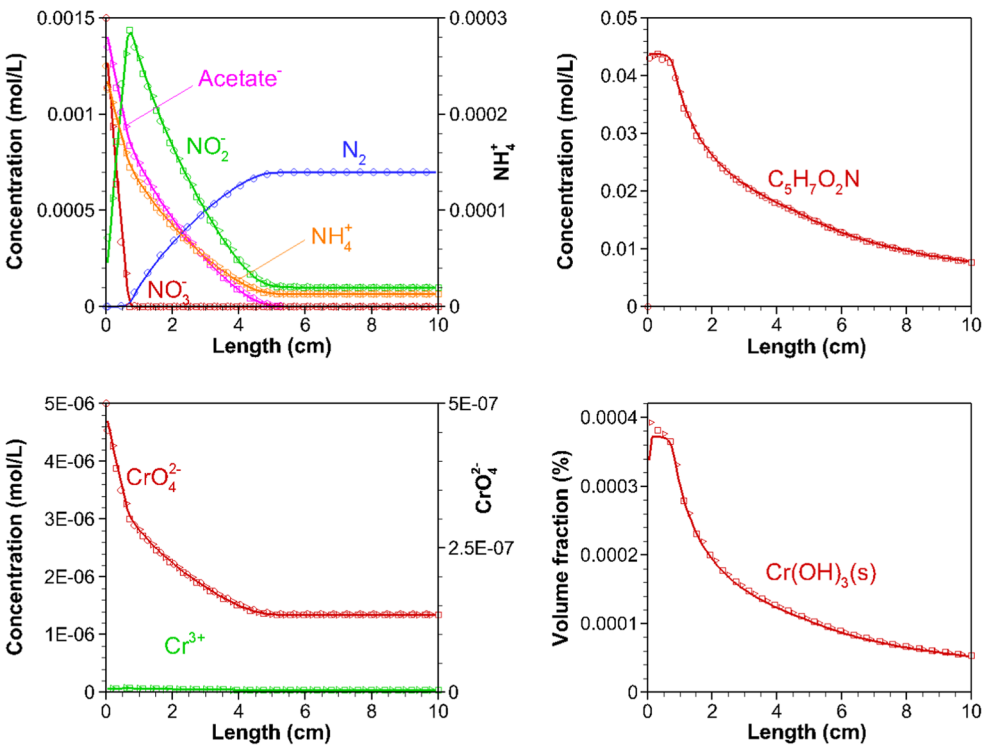


**Fig. 4** Concentration of major components in the simulation of Cr(VI) reduction under denitrifying conditions in a flow-through column with biomass growth along the length of the column at day 100 (*column 1*)

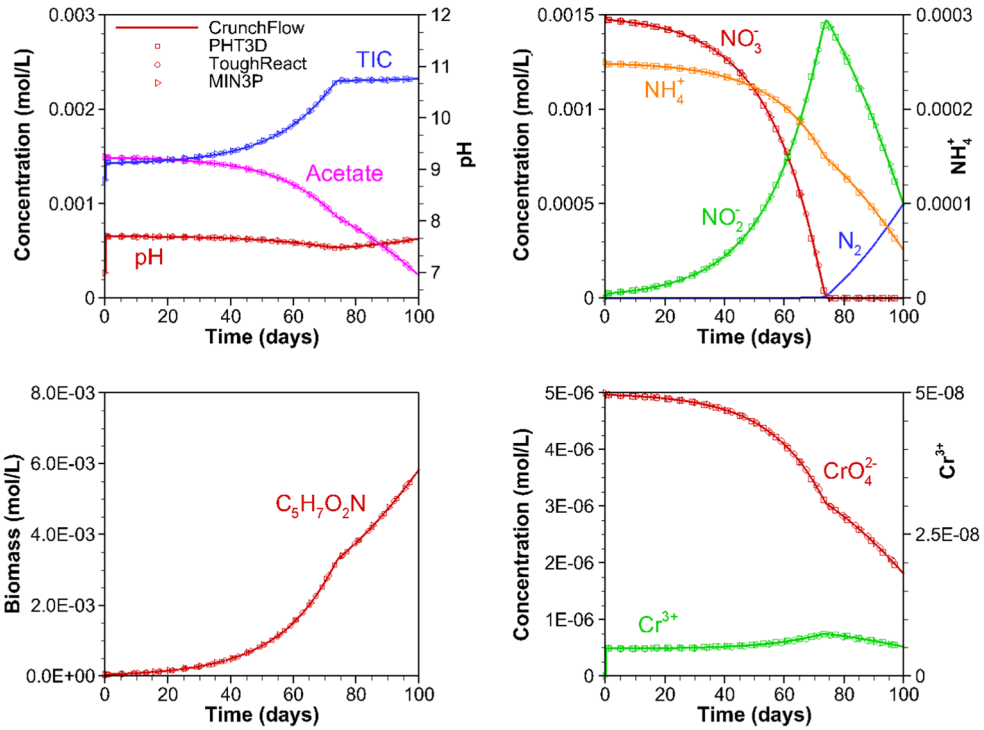


**Fig. 5** Evolution of major components in the simulation of Cr(VI) reduction under denitrifying conditions in a flow-through column with biomass growth and decay (*column 2*)

biomass concentration at 100 days is much smaller than for the case of column 1. Results from all codes agree very well as shown in Figs. 5 and 6.

Results capture qualitatively the observed and simulated evolution of effluent nitrate concentrations in the work of Clement et al. [4] (cf. Figs. 2 and 5 in [4]), where nitrate is

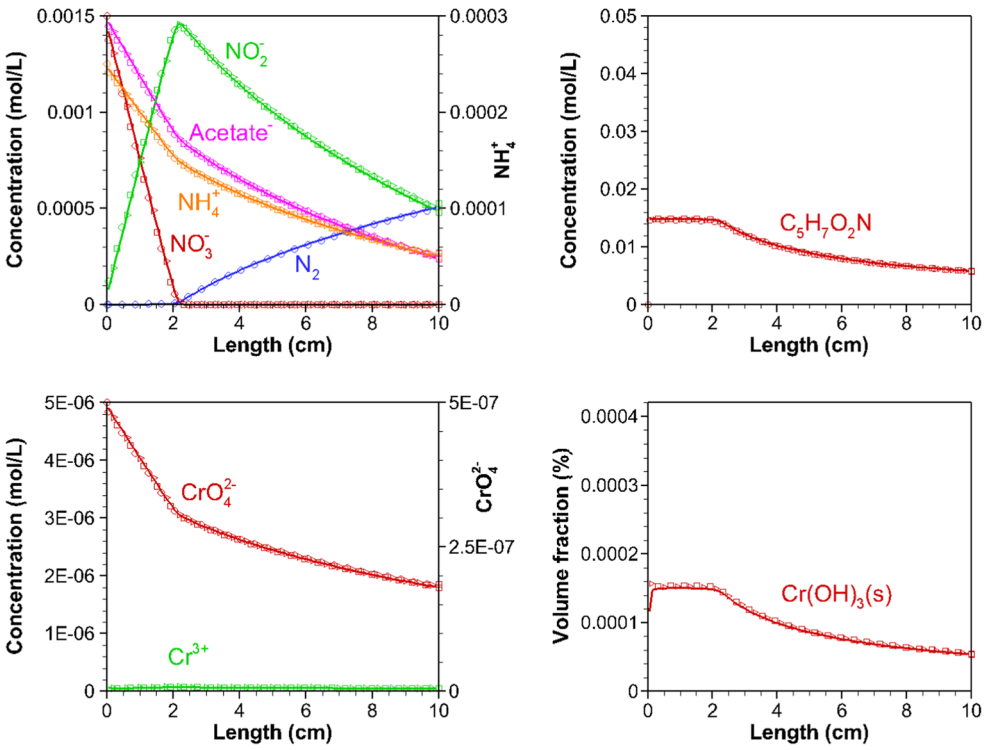


**Fig. 6** Concentration of major components in the simulation of Cr(VI) reduction under denitrifying conditions in a flow-through column with biomass growth and decay along the length of the column at day 100 (*column 2*)

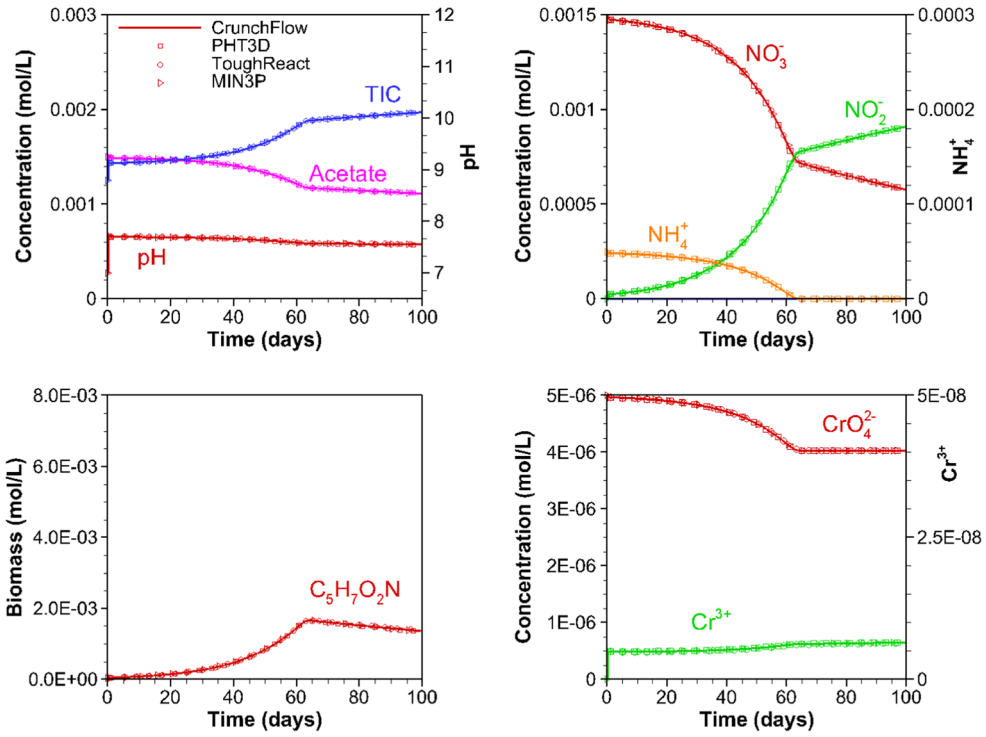


**Fig. 7** Evolution of major components in the simulation of Cr(VI) reduction under denitrifying conditions in a flow-through column with biomass growth and decay and limited $NH_4^+$ supply (*column 3*)

consumed slowly initially and then increasingly faster due to biomass growth until its complete depletion in the effluent. Direct quantitative comparison is not possible due to the differences in the parameters and the additional processes considered in [4] such as detachment and reattachment of biomass to the solid phase.

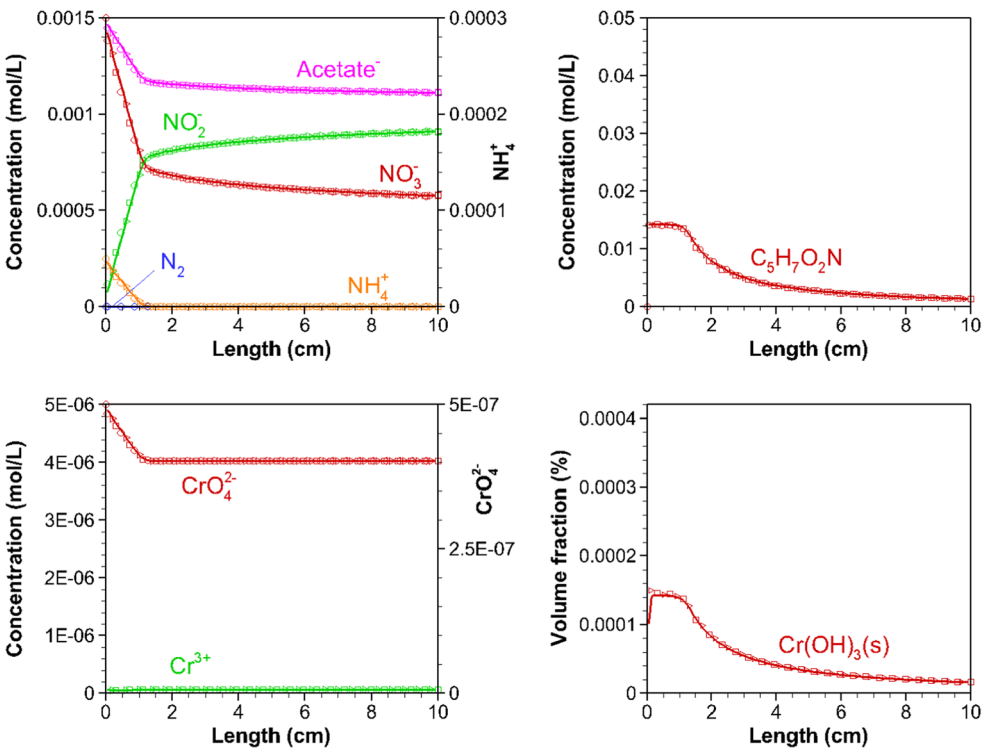


**Fig. 8** Concentration of major components in the simulation of Cr(VI) reduction under denitrifying conditions in a flow-through column with biomass growth and decay and limited $NH_4^+$ supply (*column 3*), along the length of the column at day 100

### 5.5 Principal problem (*column 3*)

By lowering the concentration of $NH_4^+$ fed to the column, the microbially mediated reactions are not limited by the availability of electron donor (e.g. as in *column 1*) or the electron acceptor, but rather by the availability of a nitrogen source for biomass growth. As a result, microorganisms need to switch to using $NO_2^-$ (R7, R8, Table 1). The rate constants for the assimilatory pathways are set to a smaller value to simulate a less favorable process. As a result, at around day 60, when $NH_4^+$ is depleted in the column, effective reaction rates are slower than under dissimilatory conditions. Because of the slower rates, $NO_3^-$ is not depleted and $NO_2^-$ is not used as electron acceptor. However, it is used as nitrogen source for biomass growth. The lower effective rates in the column are also caused by a decrease in biomass concentrations because assimilatory processes cannot sustain the biomass concentrations at the same level as dissimilatory pathways did. As an example, biomass in the outlet cell (Fig. 7) decreases after day 60 due to fast decay rates. Assimilatory pathways at day 100 still account for most of Cr(VI) reduction as can be seen in Fig. 8, where in the 1 cm near the inlet of the column, $NH_4^+$ is available.

### 5.6 Numerical performance

The relatively simple geometry of the simulation domain and the limited complexity of the reaction network proposed in this benchmark imply that simulation times for most codes fall within a relatively small range of values (120 to 200 s for the principal problem), even if the simulations were performed separately by each of the authors on different computers (clock speeds between 2.0 and 3.4 GHz), with codes using different solution approaches (Table 2) and built with different compilers and optimization levels (-O1, -O2, -O3). Simulations statistics for these runs show that non-linear (Newton) iterations per time step are similar for all codes (from 2.2 to 4.3) regardless of the solution approach (GIA or OS). A relative large number of reaction time steps were specified for the PHREEQC geochemistry engine used by PHT3D, which resulted in larger overall simulation times that are not directly comparable to the other simulators. A more rigorous evaluation of the performance of each code was deemed beyond the scope of this work and was not pursued further.

## 6 Summary and conclusions

A benchmark problem set has been developed for microbially mediated reactions that focused on the dynamics of biomass growth and decay. This problem set simulates chromium reduction under denitrifying conditions in batch and flow-through column experiments stimulated with acetate under different assumptions. These assumptions were presented as five different problem components, which were used to test specific model features while evaluating the impact of these assumptions in the model.

Microbially mediated rate expressions were based on the Monod formulation where a first-order dependence on biomass explicitly incorporated the contribution of changing biomass concentrations to the rates. Biomass played a double role, in that it was also included as a reactant in the overall microbially mediated reaction stoichiometry. This was done by considering that a portion of electron equivalents from the oxidation of acetate was used for biomass growth in the anabolic pathway. Biomass decay was incorporated using a first-order dependence on the biomass concentration. In addition, the processes of equilibrium complexation and kinetic mineral dissolution-precipitation were included in the model. Inclusion of these processes was necessary to capture correctly immobilization of chromium as $Cr(OH)_3$.

In batch simulations, biomass growth resulted in faster rates, increased use of acetate, but relatively decreased use of $NO_3^-$ and $NO_2^-$. In column simulations, biomass growth and accumulation were positive feedback mechanisms. Effective rates in the column increased over time due to an increase of microbial activity near the inlet end of the column, while the outlet end became inactive due to complete depletion of the electron donor, acceptor, or the nitrogen source for biomass growth. Inclusion of biomass decay reduced the increase in effective rates and also resulted in slower rates due to decreasing biomass concentrations in nutrient-limited regions of the column.

To ensure that the results presented in this paper were the correct solutions to the problems posed, four different general-purpose reactive transport codes were used for the simulations: CrunchFlow, PH3TD, ToughReact, and MIN3P. Modelers seeking to incorporate microbially mediated reactions into their codes will find in this problem set a simple benchmark to verify their codes that is based on well-established reaction rate formulations and sound mass balance principles.

**Acknowledgments** This work was supported as part of the Subsurface Science Scientific Focus Area funded by the U.S. Department of Energy, Office of Science, Office of Biological and Environmental Research under Award Number DE-AC02-05CH11231 (S.M. and C.W.). Funding for this research was also provided by the Natural Sciences and Engineering Research Council (NSERC) of Canada through a Discovery Grant (DG) and a Discovery Accelerator Supplement (DAS) Award held by K. U. Mayer.

## Appendix

### Section A: Geochemical system and rates

**Table 3** Primary (component) species and ion radii for Debye-Huckel model

| Number | Species | Ion radius |
|---|---|---|
| C0 | $H_2O$ | 3.0 |
| C1 | $H^+$ | 9.0 |
| C2 | $Na^+$ | 4.0 |
| C3 | $Ca^{++}$ | 6.0 |
| C4 | $Cl^-$ | 3.0 |
| C5 | $HCO_3^-$ | 4.0 |
| C6 | Acetate | 4.5 |
| C7 | $NO_3^-$ | 3.0 |
| C8 | $NO_2^-$ | 3.0 |
| C9 | $N_2$(aq) | 3.0 |
| C10 | $NH_4^+$ | 2.5 |
| C11 | $O_2$(aq) | 3.0 |
| C12 | $CrO_4^{--}$ | 4.0 |
| C13 | $Cr^{+++}$ | 9.0 |
| C14 | $C_5H_7O_2N$ | N/A |

**Table 4** Aqueous complexation reactions and ion radii for corresponding

| Number | Species | log $K$ | Primary species stoichiometric coefficients | | | | | | | | | | | | | | Ion |
|---|---|---|---|---|---|---|---|---|---|---|---|---|---|---|---|---|---|
| | | | $H^+$ | $Na^+$ | $Ca^{++}$ | $Cl^-$ | $HCO_3^-$ | $Acetate^-$ | $NO_3^-$ | $NO_2^-$ | $N_2$(aq) | $NH_4^+$ | $O_2$(aq) | $CrO_4^{--}$ | $Cr^{+++}$ | $C_5H_7O_2N$ | radius |
| A1 | $OH^-$ | 13.991 | −1 | 0 | 0 | 0 | 0 | 0 | 0 | 0 | 0 | 0 | 0 | 0 | 0 | 0 | 3.5 |
| A2 | $CO_2$(aq) | −6.341 | 1 | 0 | 0 | 0 | 1 | 0 | 0 | 0 | 0 | 0 | 0 | 0 | 0 | 0 | 3.0 |
| A3 | $CO_3^{--}$ | 10.325 | −1 | 0 | 0 | 0 | 1 | 0 | 0 | 0 | 0 | 0 | 0 | 0 | 0 | 0 | 4.5 |
| A4 | $CaOH^+$ | 12.850 | −1 | 0 | 1 | 0 | 0 | 0 | 0 | 0 | 0 | 0 | 0 | 0 | 0 | 0 | 4.0 |
| A5 | $CaCO_3$(aq) | 7.009 | −1 | 0 | 1 | 0 | 1 | 0 | 0 | 0 | 0 | 0 | 0 | 0 | 0 | 0 | 3.0 |
| A6 | $CaCl^+$ | 0.700 | 0 | 0 | 1 | 1 | 0 | 0 | 0 | 0 | 0 | 0 | 0 | 0 | 0 | 0 | 4.0 |
| A7 | $CaHCO_3^+$ | −1.043 | 0 | 0 | 1 | 0 | 1 | 0 | 0 | 0 | 0 | 0 | 0 | 0 | 0 | 0 | 4.0 |
| A8 | $CaCH_3COO^+$ | −0.928 | 0 | 0 | 1 | 0 | 0 | 1 | 0 | 0 | 0 | 0 | 0 | 0 | 0 | 0 | 4.0 |
| A9 | $Ca(CH_3COO)_2$ | −2.127 | 0 | 0 | 1 | 0 | 0 | 2 | 0 | 0 | 0 | 0 | 0 | 0 | 0 | 0 | 3.0 |
| A10 | $NH_3$(aq) | 46.871 | 1 | 0 | 0 | 0 | 0 | 0 | 0 | 1 | 0 | 0 | −1.5 | 0 | 0 | 0 | 3.0 |
| A11 | $Cr(OH)_2^+$ | 9.700 | −2 | 0 | 0 | 0 | 0 | 0 | 0 | 0 | 0 | 0 | 0 | 0 | 1 | 0 | 4.0 |
| A12 | $Cr(OH)_3$(aq) | 18.000 | −3 | 0 | 0 | 0 | 0 | 0 | 0 | 0 | 0 | 0 | 0 | 0 | 1 | 0 | 3.0 |
| A13 | $Cr(OH)_4^-$ | 27.400 | −4 | 0 | 0 | 0 | 0 | 0 | 0 | 0 | 0 | 0 | 0 | 0 | 1 | 0 | 4.0 |
| A14 | $Cr_2(OH)_2^{++++}$ | 5.060 | −2 | 0 | 0 | 0 | 0 | 0 | 0 | 0 | 0 | 0 | 0 | 0 | 2 | 0 | 4.0 |
| A15 | $Cr_2O_7^{--}$ | −14.511 | 2 | 0 | 0 | 0 | 0 | 0 | 0 | 0 | 0 | 0 | 0 | 2 | 0 | 0 | 4.0 |
| A16 | $Cr_3(OH)_4$(5+) | 8.150 | −4 | 0 | 0 | 0 | 0 | 0 | 0 | 0 | 0 | 0 | 0 | 0 | 3 | 0 | 6.0 |
| A17 | $CrCl^{++}$ | 0.149 | 0 | 0 | 0 | 1 | 0 | 0 | 0 | 0 | 0 | 0 | 0 | 0 | 1 | 0 | 4.5 |
| A18 | $CrCl_2^+$ | −0.148 | 0 | 0 | 0 | 2 | 0 | 0 | 0 | 0 | 0 | 0 | 0 | 0 | 1 | 0 | 4.0 |
| A19 | $CrOH^{++}$ | 4.000 | −1 | 0 | 0 | 0 | 0 | 0 | 0 | 0 | 0 | 0 | 0 | 0 | 1 | 0 | 4.5 |
| A20 | Acetic_acid(aq) | −4.752 | 1 | 0 | 0 | 0 | 0 | 1 | 0 | 0 | 0 | 0 | 0 | 0 | 0 | 0 | 3.0 |

*Stoichiometric coefficients for products $> 0$ and for reactants $< 0$

**Table 5** Minerals

| Number | Mineral | log $K$ | Primary species | | | | | | | | | | | |
|---|---|---|---|---|---|---|---|---|---|---|---|---|---|---|
| | | | $H^+$ | $Na^+$ | $Ca^{++}$ | $Cl^-$ | $HCO_3^-$ | $Acetate^-$ | $NO_3^-$ | $NO_2^-$ | $N_2(aq)$ | $NH_4^+$ | $O_2(aq)$ | $CrO_4^{--}$ | $Cr^{+++}$ |
| M1 | $Cr(OH)_3(s)$ | 8.9500 | −3 | 0 | 0 | 0 | 0 | 0 | 0 | 0 | 0 | 0 | 0 | 0 | 1 |
| M2 | Calcite | 1.8542 | −1 | 0 | 1 | 0 | 1 | 0 | 0 | 0 | 0 | 0 | 0 | 0 | 0 |

*Stoichiometric coefficients for products > 0 and for reactants < 0

**Table 6** Stoichiometry of microbially mediated reactions (Table 1 in manuscript)

| Number | Reaction | Primary species | | | | | | | | | |
|---|---|---|---|---|---|---|---|---|---|---|---|
| | | $H^+$ | $HCO_3^-$ | Acetate | $NO_3^-$ | $NO_2^-$ | $N_2(aq)$ | $NH_4^+$ | $CrO_4^{--}$ | $Cr^{+++}$ | $C_5H_7O_2N$ |
| R1 | Catabolic | | | | | | | | | | |
| | $NO_3^- \rightarrow NO_2^-$ | 0.125 | 0.25 | −0.125 | −0.5 | 0.5 | 0 | 0 | 0 | 0 | 0 |
| R2 | Catabolic | | | | | | | | | | |
| | $NO_2^- \rightarrow N_2(aq)$ | −0.20833 | 0.25 | −0.125 | 0 | −0.33333 | 0.166667 | 0 | 0 | 0 | 0 |
| R3 | Anabolic – dissiml. | | | | | | | | | | |
| | Acetate $\rightarrow C_5H_7O_2N$ | −0.075 | 0 | −0.125 | 0 | 0 | 0 | −0.050 | 0 | 0 | 0.050 |
| R4 | Anabolic – assimil. | | | | | | | | | | |
| | Acetate $\rightarrow C_5H_7O_2N$ | −0.105769 | 0.057692 | −0.125 | 0 | −0.038461 | 0 | 0 | 0 | 0 | 0.038461 |
| R5 | Overall fe = 0.6 | | | | | | | | | | |
| | $NO_3^- \rightarrow NO_2^-$ | 0.045 | 0.15 | −0.125 | −0.3 | 0.3 | 0 | −0.02 | 0 | 0 | 0.02 |
| R6 | Overall fe = 0.6 | | | | | | | | | | |
| | $NO_2^- \rightarrow N_2(aq)$ | −0.155 | 0.15 | −0.125 | 0 | −0.2 | 0.1 | −0.02 | 0 | 0 | 0.02 |
| R7 | Overall fe = 0.6 | | | | | | | | | | |
| | Assimilatory | | | | | | | | | | |
| | $NO_3^- \rightarrow NO_2^-$ | 0.032692 | 0.173077 | −0.125 | −0.3 | 0.284615 | 0 | 0 | 0 | 0 | 0.015385 |
| R8 | Overall fe = 0.6 | | | | | | | | | | |
| | Assimilatory | | | | | | | | | | |
| | $NO_2^- \rightarrow N_2(aq)$ | −0.167308 | 0.173077 | −0.125 | 0 | −0.215385 | 0.1 | 0 | 0 | 0 | 0.015385 |
| R9 | Cr reduction | | | | | | | | | | |
| | $(NO_3^-)$ | −1.54167 | 0.25 | −0.125 | 0 | 0 | 0 | 0 | −0.33333 | 0.333333 | 0 |
| R10 | Cr reduction | | | | | | | | | | |
| | $(NO_2^-)$ | −1.54167 | 0.25 | −0.125 | 0 | 0 | 0 | 0 | −0.33333 | 0.333333 | 0 |

Stoichiometric coefficients for products > 0 and for reactants < 0

**Table 7** Rate constants and kinetic parameters for microbially mediated reactions

| Number | Aqueous kinetics | Rate constant | Monod term half saturations | | | | | Inhibition half saturation | |
|---|---|---|---|---|---|---|---|---|---|
| | | | $Acetate^-$ | $NO_3^-$ | $NO_2^-$ | $CrO_4^{2-}$ | $NH_4^+$ | $NO_3^-$ | $NH_4^+$ |
| | | mol $cell^{-1}$ $s^{-1}$ | mol $L^{-1}$ | mol $L^{-1}$ | mol $L^{-1}$ | mol $L^{-1}$ | mol $L^{-1}$ | mol $L^{-1}$ | mol $L^{-1}$ |
| R1 | Catabolic | | | | | | | | |
| | $NO_3^- \rightarrow NO_2^-$ | $8 \times 10^{-20}$ | 2.03E−5 | 1.06E−5 | | | 1E−6 | | |
| R2 | Catabolic | | | | | | | | |
| | $NO_2^- \rightarrow N_2$(aq) | $4 \times 10^{-20}$ | 2.03E−5 | | 1.06E−5 | | 1E−6 | 1.06E−5 | |
| R3 | Anabolic | | | | | | | | |
| | Acetate $\rightarrow C_5H_7O_2N$ | | | | | | | | |
| R4 | Anabolic($NO_2^-$) | | | | | | | | |
| | Acetate $\rightarrow C_5H_7O_2N$ | | | | | | | | |
| R5 | Overall fe = 0.6 | | | | | | | | |
| | $NO_3^- \rightarrow NO_2^-$ | $8 \times 10^{-20}$ | 2.03E−5 | 1.06E−5 | | | 1E−6 | | |
| R6 | Overall fe = 0.6 | | | | | | | | |
| | $NO_2^- \rightarrow N_2$(aq) | $4 \times 10^{-20}$ | 2.03E−5 | | 1.06E−5 | | 1E−6 | 1.06E−5 | |
| R7 | Overall fe = 0.6 | | | | | | | | |
| | Assimilatory | | | | | | | | |
| | $NO_3^- \rightarrow NO_2^-$ | $8 \times 10^{-21}$ | 2.03E−5 | 1.06E−5 | | | | | 1.06E−5 |
| R8 | Overall fe = 0.6 | | | | | | | | |
| | Assimilatory | | | | | | | | |
| | $NO_2^- \rightarrow N_2$(aq) | $4 \times 10^{-21}$ | 2.03E−5 | | 1.06E−5 | | 1E−6 | 1.06E−5 | 1.06E−5 |
| R9 | Cr reduction ($NO_3^-$) | $9.513 \times 10^{-23}$ | 2.03E−5 | 1.06E−5 | | 1E−7 | 1E−6 | | |
| R10 | Cr reduction ($NO_2^-$) | $3.171 \times 10^{-23}$ | 2.03E−5 | | 1.06E−5 | 1E−7 | 1E−6 | 1.06E−5 | |

**Table 8** Rate constants and kinetic parameters for mineral reactions

| *m* | Mineral | Rate constant | Notes |
|---|---|---|---|
| 1 | $Cr(OH)_3$(s) | $2.5 \times 10^{-9}$ mol $m^{-2}$ $s^{-1}$ | Batches 1 and 2 |
| 1 | $Cr(OH)_3$(s) | $10^{-9}$ mol $m^{-2}$ $s^{-1}$ | Columns 1, 2, and 3 |
| 2 | $C_5H_7O_2N$(s) | $10^{2}$ mol $m^{-3}$ $s^{-1}$ | Arbitrarily fast |
| 3 | Calcite | $10^{-5.18}$ | |
| 4 | Decay_$C_5H_7O_2N$ | 0.00432 $day^{-1}$ | |

**Table 9** Debye-Huckel* parameters at 25 °C

| Parameters | Value |
|---|---|
| A | 0.5114 |
| B | 0.3288 |
| b | 0.0410 |

*Debye-Huckel model for activity of species: $log\gamma_i = -\frac{Az_i^2 I^{\frac{1}{2}}}{1+B\dot{a}_i I^{\frac{1}{2}}} + bI$, where $\gamma_i$ is the activity coefficient of species $i$, $Z_i$ is the charge, and $\dot{a}_i$ is the ion radius. The ionic strength is denoted with $I$

## Section B: Geochemical conditions

**Table 10** Geochemical conditions for batch and column simulation Parameters

| Parameter | Batch simulations | Column simulations |
|---|---|---|
| Temperature (C) | 25 | 25 |
| Porosity | 0.4 | 0.4 |
| Liquid saturation | 1 | 1 |
| Liquid density (kg/$m^3$) | 1,000 | 1,000 |
| Solid density (kg/$m^3$) | 90.4 | 2,709.238 |
| Solid:solution ratio | 135.601 | 4,063.858 |
| Ionic strength | 0.01 | 0.01 |
| Solution pH | 7 | 7 |
| Total charge | −2.63E−18 | −6.88E−19 |

**Table 11** Total concentrations in molality (mol/Kgw)

| Components | Batch simulations | Column simulations |
|---|---|---|
| $H^+$ | 2.07E−04 | 2.10E−04 |
| $Na^+$ | 5.25E−03 | 5.25E−03 |
| $Ca^{++}$ | 1.60E−03 | 1.60E−03 |
| $Cl^-$ | 4.95E−03 | 4.45E−03 |
| $HCO_3^-$ | 1.25E−03 | 1.25E−03 |
| Acetate | 1.00E−03 | 1.50E−03 |
| $NO_3^-$ | 1.50E−03 | 1.50E−03 |
| $NO_2^-$ | 1.00E−33 | 1.00E−33 |
| $N_2$(aq) | 1.00E−33 | 1.00E−33 |
| $NH_4^+$ | 2.50E−04 | 2.50E−04 |
| $O_2$(aq) | 1.00E−13 | 1.00E−13 |
| $CrO_4^{--}$ | 5.00E−06 | 5.00E−06 |
| $Cr^{+++}$ | 1.00E−33 | 1.00E−33 |
| $C_5H_7O_2N$ | 1.00E−04 | 5.00E−05 |

**Table 12** Species concentrations (mol/Kgw) and activities

| Species | Batch simulations | | | Column simulations | | |
|---|---|---|---|---|---|---|
| | Molality | Activity | Activity coefficient | Molality | Activity | Activity coefficient |
| $H^+$ | 1.10E−07 | 1.00E−07 | 9.13E−01 | 1.10E−07 | 1.00E−07 | 9.13E−01 |
| $Na^+$ | 5.25E−03 | 4.73E−03 | 9.01E−01 | 5.25E−03 | 4.73E−03 | 9.01E−01 |
| $Ca^{++}$ | 1.58E−03 | 1.06E−03 | 6.73E−01 | 1.57E−03 | 1.06E−03 | 6.73E−01 |
| $Cl^-$ | 5.15E−03 | 4.62E−03 | 8.98E−01 | 4.65E−03 | 4.18E−03 | 8.98E−01 |
| $HCO_3^-$ | 1.03E−03 | 9.31E−04 | 9.01E−01 | 1.03E−03 | 9.31E−04 | 9.01E−01 |
| Acetate | 9.86E−04 | 8.90E−04 | 9.03E−01 | 1.48E−03 | 1.34E−03 | 9.03E−01 |
| $NO_3^-$ | 1.50E−03 | 1.35E−03 | 8.98E−01 | 1.50E−03 | 1.35E−03 | 8.98E−01 |
| $NO_2^-$ | 1.00E−33 | 8.98E−34 | 8.98E−01 | 1.00E−33 | 8.98E−34 | 8.98E−01 |
| $N_2$(aq) | 1.00E−33 | 1.00E−33 | 1.00E+00 | 1.00E−33 | 1.00E−33 | 1.00E+00 |
| $NH_4^+$ | 2.50E−04 | 2.24E−04 | 8.97E−01 | 2.50E−04 | 2.24E−04 | 8.97E−01 |
| $O_2$(aq) | 1.00E−13 | 1.00E−13 | 1.00E+00 | 1.00E−13 | 1.00E−13 | 1.00E+00 |
| $CrO_4^{--}$ | 5.00E−06 | 3.29E−06 | 6.58E−01 | 5.00E−06 | 3.29E−06 | 6.58E−01 |
| $Cr^{+++}$ | 9.24E−38 | 4.06E−38 | 4.39E−01 | 9.23E−38 | 4.06E−38 | 4.39E−01 |
| $C_5H_7O_2N$ | 1.00E−4 | 1.00E−4 | 1.00E+00 | 5.00E−5 | 5.00E−5 | 1.00E+00 |
| $OH^-$ | 1.13E−07 | 1.02E−07 | 9.00E−01 | 1.13E−07 | 1.02E−07 | 9.00E−01 |
| $CO_2$(aq) | 2.04E−04 | 2.04E−04 | 1.00E+00 | 2.04E−04 | 2.04E−04 | 1.00E+00 |
| $CO_3^{--}$ | 6.66E−07 | 4.40E−07 | 6.62E−01 | 6.66E−07 | 4.40E−07 | 6.62E−01 |
| $CaOH^+$ | 1.66E−09 | 1.50E−09 | 9.01E−01 | 1.66E−09 | 1.50E−09 | 9.01E−01 |
| $CaCO_3$(aq) | 9.66E−07 | 9.68E−07 | 1.00E+00 | 9.63E−07 | 9.66E−07 | 1.00E+00 |
| $CaCl^+$ | 1.09E−06 | 9.78E−07 | 9.01E−01 | 9.78E−07 | 8.82E−07 | 9.01E−01 |
| $CaHCO_3^+$ | 1.21E−05 | 1.09E−05 | 9.01E−01 | 1.21E−05 | 1.09E−05 | 9.01E−01 |
| $CaCH_3COO^+$ | 8.87E−06 | 8.00E−06 | 9.01E−01 | 1.33E−05 | 1.20E−05 | 9.01E−01 |
| $Ca(CH_3COO)_2$(aq) | 1.12E−07 | 1.13E−07 | 1.00E+00 | 2.52E−07 | 2.53E−07 | 1.00E+00 |
| $NH_3$(aq) | 3.80E−68 | 3.81E−68 | 1.00E+00 | 3.80E−68 | 3.81E−68 | 1.00E+00 |
| $Cr(OH)_2^+$ | 8.98E−34 | 8.09E−34 | 9.01E−01 | 8.98E−34 | 8.09E−34 | 9.01E−01 |
| $Cr(OH)_3$(aq) | 4.05E−35 | 4.06E−35 | 1.00E+00 | 4.05E−35 | 4.06E−35 | 1.00E+00 |
| $Cr(OH)_4^-$ | 1.79E−37 | 1.62E−37 | 9.01E−01 | 1.79E−37 | 1.62E−37 | 9.01E−01 |
| $Cr_2(OH)_2^{++++}$ | 7.15E−66 | 1.43E−66 | 2.00E−01 | 7.15E−66 | 1.43E−66 | 2.00E−01 |
| $Cr_2O_7^{--}$ | 5.33E−11 | 3.50E−11 | 6.58E−01 | 5.33E−11 | 3.51E−11 | 6.58E−01 |
| $Cr_3(OH)_4(5+)$ | 5.63E−92 | 4.72E−93 | 8.39E−02 | 5.63E−92 | 4.72E−93 | 8.40E−02 |
| $CrCl^{++}$ | 2.01E−40 | 1.33E−40 | 6.62E−01 | 1.82E−40 | 1.20E−40 | 6.62E−01 |
| $CrCl_2^+$ | 1.35E−42 | 1.22E−42 | 9.01E−01 | 1.10E−42 | 9.94E−43 | 9.01E−01 |
| $CrOH^{++}$ | 6.13E−35 | 4.06E−35 | 6.62E−01 | 6.13E−35 | 4.06E−35 | 6.62E−01 |
| Acetic_acid(aq) | 5.01E−06 | 5.02E−06 | 1.00E+00 | 7.52E−06 | 7.53E−06 | 1.00E+00 |

**Table 13** Minerals and parameters

| | | | | |
|---|---|---|---|---|
| $Cr(OH)_3(s)$ | Initial volume fraction | 1.00E−10 | specific_surface_area | 1.00E+04 $m^2/g$ |
| Calcite | Initial volume fraction | 0.1 | bulk_surface_area | 100 $m^2/m^3$ bulk |

For $Cr(OH)_3(s)$,

$A_{\text{specific}} = 10^4\ \text{m}^2\text{g}^{-1}, \quad \text{MW} = 103.0181\ \text{g} \cdot \text{mol}^{-1}, \quad V_m = 11.1\ \text{cm}^3\ \text{mol}^{-1}, \quad \varphi_{\text{init}} = 10^{-10}\ \text{m}^3\ \text{mineral} \cdot \text{m}^{-3}\ \text{bulk}$

$$A_{\text{bulk}} = A_{\text{specific}} \frac{\varphi_{\text{init}} \text{MW}}{V_m} = 9.281\ \text{m}^2\ \text{mineral} \cdot\ \text{m}^{-3}\ \text{bulk}$$

## Section C: Biomass unit conversion

**Table 14** Biomass unit conversion

| Parameter | Value |
|---|---|
| Carbon in biomass per cell | $10^{-14}$ mol C $cell^{-1}$ |
| Mass of a cell ($C_5H_7O_2N$) | $2 \times 10^{-15}$ mol $C_5H_7O_2N$ $cell^{-1}$ |
| Volume of a cell | 1 $\mu m^3$ $cell^{-1}$ = $10^{-18}$ $m^3$ $cell^{-1}$ |
| Volume per mol of $C_5H_7O_2N$ | 500 $cm^3$ $mol^{-1}$ $C_5H_7O_2N$ |

## References


1. André, L., Pauwels, H., Dictor, M.-C., Parmentier, M., Azaroual, M.: Experiments and numerical modelling of microbially-catalysed denitrification reactions. Chem. Geol. **287**(3-4), 171–181 (2011)
2. Beller, H.R., Yang, L., Varadharajan, C., Han, R., Lim, H., Karaoz, U., Molins, S., Marcus, M.A., Brodie, E.L., Steefel, C.I., Nico, P.S.: Divergent aquifer biogeochemical systems converge on similar and unexpected Cr(VI) reduction products. Environ. Sci. Technol. (2014). doi:10.1021/es5016982
3. Brodie, E.L., Joyner, D.C., Faybishenko, B., Conrad, M.E., Rios-Velazquez, C., Malave, J., Martinez, R., Mork, B., Willett, A., Koenigsberg, S., Herman, D.J., Firestone, M.K., Hazen, T.C.: Microbial community response to addition of polylactate compounds to stimulate hexavalent chromium reduction in groundwater. Chemosphere **85**(4), 660–665 (2011)
4. Clement, T., Peyton, B., Skeen, R., Jennings, D., Petersen, J.: Microbial growth and transport in porous media under denitrification conditions: experiments and simulations. J. Contam. Hydrol. **24**(3-4), 269–285 (1997)
5. Druhan, J.L., Conrad, M.E., Williams, K.H., N'Guessan, L., Long, P.E., Hubbard, S.S.: Sulfur isotopes as indicators of amended bacterial sulfate reduction processes influencing field scale uranium bioremediation. Environ. Sci. & Technol. **42**(21), 7842–7849 (2008)
6. Druhan, J.L., Steefel, C.I., Molins, S., Williams, K.H., Conrad, M.E., DePaolo, D.J.: Timing the onset of sulfate reduction over multiple subsurface acetate amendments by measurement and modeling of sulfur isotope fractionation. Environ. Sci. & Technol. **46**(16), 8895–8902 (2012)
7. Faybishenko, B., Hazen, T.C., Long, P.E., Brodie, E.L., Conrad, M. E., Hubbard, S.S., Christensen, J.N., Joyner, D., Borglin, S. E., Chakraborty, R., Williams, K.H., Peterson, J. E., Chen, J., Brown, S.T., Tokunaga, T.K., Wan, J., Firestone, M., Newcomer, D.R., Resch, C.T., Cantrell, K.J., Willett, A., Koenigsberg, S.: In situ long-term reductive bioimmobilization of Cr(VI) in groundwater using hydrogen release compound. Environ. Sci. & Technol. **42**(22), 8478–8485 (2008)
8. Gupta, A., Lake, L., Pope, G., Sepehrnoori, K., King, M.: High-resolution monotonic schemes for reservoir fluid-flow simulation. In Situ **15**(3), 289–317 (1991)
9. Han, R., Geller, J.T., Yang, L., Brodie, E.L., Chakraborty, R., Larsen, J.T., Beller, H.R.: Physiological and Transcriptional Studies of Cr(VI) Reduction under aerobic and denitrifying conditions by an aquifer-derived pseudomonad. Environ. Sci. & Technol. **44**(19), 7491–7497 (2010)
10. Li, L., Steefel, C.I., Kowalsky, M.B., Englert, A., Hubbard, S.S.: Effects of physical and geochemical heterogeneities on mineral transformation and biomass accumulation during biostimulation experiments at Rifle, Colorado. J. Contam. Hydrol. **112**(1–4), 45–63 (2010)
11. Li, L., Steefel, C.I., Williams, K.H., Wilkins, M.J., Hubbard, S.S.: Mineral transformation and biomass accumulation associated with uranium bioremediation at Rifle, Colorado. Environ. Sci. & Technol. **43**(14), 5429–5435 (2009)
12. Lichtner, P.C.: Continuum model for simultaneous chemical reactions and mass transport in hydrothermal systems. Geochimica et Cosmochimica Acta **49**(3), 779–800 (1985)
13. Mayer, K., Amos, R.T., Molins, S., Gerard, F.: Reactive transport modeling in variably saturated media with MIN3P: basic model formulation and model enhancements, 186–211: Groundwater reactive transport models, ground water reactive transport model (2012)
14. Mayer, K.U., Frind, E.O., Blowes, D.W.: Multicomponent reactive transport modeling in variably saturated porous media using a generalized formulation for kinetically controlled reactions. Water Resour. Res. **38**(9), 13–1–13–21 (2002)
15. Prommer, H., Barry, D., Zheng, C.: MODFLOW/MT3DMS-based reactive multicomponent transport modeling. Ground Water **41**(2), 247–257 (2003)
16. Rai, D., Sass, B.M., Moore, D.A.: Chromium(III) hydrolysis constants and solubility of chromium(III) hydroxide. Inorg. Chem. **26**(3), 345–349 (1987)

17. Rittmann, B., McCarty, P.: Environmental biotechnology: principles and applications, McGraw-Hill series in water resources and environmental engineering. McGraw-Hill, London (2001)
18. Steefel, C., MacQuarrie, K.: Approaches to modeling of reactive transport in porous media. In: Lichtner, P.C., Steefel, C.I., Oelkers, E.H. (eds.) Reactive transport in porous media, reviews in mineralogy, Vol. 34, 83–129, Mineral Soc Amer, Mineralogical Soc America, 1130 Seventeenth St Nw, Suite 330, Washington, DC 20036, Short Course on Reactive Transport in Porous Media, GOLDEN, CO, OCT 25-27, 1996 (1996)
19. Steefel, C.I., Lasaga, A.C.: A coupled model for transport of multiple chemical species and kinetic precipitation/dissolution reactions with application to reactive flow in single phase hydrothermal systems. American Journal of Science **294**(5), 529–592 (1994)
20. Steefel, C.I., Appelo, C.A.J., Arora, B., Jacques, D., Kalbacher, T., Kolditz, O., Lagneau, V., Lichtner, P.C., Mayer, K.U., Meussen, H., Molins, S., Moulton, D., Parkhurst, D.L., Shao, H., Simunek, J., Spycher, N., Yabusaki, S., Yeh, G.T.: Reactive transport codes for subsurface environmental simulation. Comput. Geosci. (2014). doi:10.1007/s10596-014-9443-x
21. Unger, A., Forsyth, P., Sudicky, E.: Variable spatial and temporal weighting schemes for use in multi-phase compositional problems. Adv. Water Resour. **19**(1), 1–27 (1996)
22. Van Leer, B.: Towards the ultimate conservative difference scheme. II. Monotonicity and conservation combined in a second-order scheme. J. Comput. Phys. **14**(4), 361–370 (1974)
23. Van Rijn, J., Tal, Y., Barak, Y.: Influence of volatile fatty acids on nitrite accumulation by a pseudomonas stutzeri strain isolated from a denitrifying fluidized bed reactor. Appl. Environ. Microbiol. **62**(7), 2615–2620 (1996)
24. Williams, K.H., Kemna, A., Wilkins, M.J., Druhan, J., Arntzen, E., Nâ€™Guessan, A.L., Long, P.E., Hubbard, S.S., Banfield, J. F.: Geophysical monitoring of coupled microbial and geochemical processes during stimulated subsurface bioremediation. Environ. Sci. & Technol. **43**(17), 6717–6723 (2009)
25. Williams, K.H., Long, P.E., Davis, J.A., Wilkins, M.J., N'Guessan, A.L., Steefel, C.I., Yang, L., Newcomer, D., Spane, F.A., Kerkhof, L.J., McGuinness, L., Dayvault, R., Lovley, D.R.: Acetate availability and its influence on sustainable bioremediation of uranium-contaminated groundwater. Geomicrobiol. J. **28**(5-6), 519–539 (2011)
26. Xu, T., Sonnenthal, E., Spycher, N., Zhang, G., Zheng, L., Pruess, K.: TOUGHREACT: A simulation program for subsurface reactive chemical transport under non-isothermal multiphase flow conditions, chap. TOUGHREACT: a simulation program for subsurface reactive chemical transport under non-isothermal multiphase flow conditions, 74–95: Groundwater reactive transport models, ground water reactive transport model (2012)
27. Yabusaki, S.B., Fang, Y., Williams, K.H., Murray, C.J., Ward, A.L., Dayvault, R.D., Waichler, S.R., Newcomer, D.R., Spane, F.A., Long, P.E.: Variably saturated flow and multicomponent biogeochemical reactive transport modeling of a uranium bioremediation field experiment. J. Contam. Hydrol. **126**(3-4), 271–290 (2011)
28. Yeh, G.T., Tripathi, V.S.: A critical evaluation of recent developments in hydrogeochemical transport models of reactive multichemical components. Water Resour. Res. **25**(1), 93–108 (1989)
29. Zhang, F., Parker, J.: Groundwater reactive transport models, ground water reactive transport model. Bentham Science Publishers, Oak Park (2012)